Frequency and Stochastic Domain Models for Two Geometries of the IPS Wave Power Buoy

José J. Cândido [#1], Paulo A.P.S. Justino [*2], João C. C. Henriques[#3]

[#]*IDMEC, Instituto Superior Técnico*
Av. Rovisco Pais, 1049-001 Lisbon, Portugal
[1]jose.candido@ist.utl.pt
[3]joaochenriques@ist.utl.pt

[*] *Unidade de Energia Solar, Eólica e das Ondas, LNEG*
Estrada do Paço do Lumiar, 1649-038 Lisbon, Portugal
[2]paulo.justino@lneg.pt

***Abstract*— Frequency-domain analysis is applied to a geometry of the original IPS buoy device concept. The analysis is particularly useful in the early development stages to establish the response of power take-off mechanism characteristic parameters to different frequencies of the wave spectrum. Optimal mechanical damping and spring coefficients are computed for some parameters restrictions. Absorbed power, capture width and other variables, such as relative displacement, are computed for regular waves and these optimal mechanical coefficients.**

A stochastic model is developed in order to evaluate the IPS buoy behaviour for irregular waves' conditions. This allows defining probability density functions for parameters that characterize the device's behaviour. Assuming that the overall system behaviour is linear and that the surface elevation for irregular waves may be regarded as a stochastic process with a Gaussian probability density function, the variables that define the system behaviour, such as bodies' displacements and velocities, will also hold a Gaussian probability density function. The average power extraction is computed for different sea state conditions.

Aiming to enhance the device's hydrodynamic performance, a new non-axisymmetric IPS geometry is conceived. Using the stochastic modelling approach, the device's behaviour is studied for several wave directions and compared to the axisymmetric configuration's behaviour.

***Keywords*— Frequency-domain model, stochastic model, IPS buoy, non-axisymmetric geometry**

I. INTRODUCTION

Offshore wave energy devices enable the exploitation of higher wave energy resources in deep water sites. In many of the currently existing (or planned) offshore devices the energy extraction results from the oscillating movement of a single body reacting against a fixed frame of reference (the sea bottom or a bottom-fixed structure). The distance between the floating body and this fixed frame of reference may prove to be considerably large, so that alternative configurations should be considered in which the wave energy extraction occurs from the relative oscillating movement between two bodies with different hydrodynamic characteristics. The theoretical basis for the analysis of the hydrodynamics of such devices was established in [1].

It may be useful to adopt a configuration in which one of the bodies presents a considerably large inertia, so that it can be considered as a frame of reference in relation to which the other body moves. In this manner, the wave energy device's characteristics are closer to the ones of a single-body device, avoiding not only the constrains reffered to [2] but also the more complex control problematic associated to two-body devices [3]. In the IPS buoy, a two-body wave energy device invented in 1978 by Sven A. Noren [4], the practical and economical problems that the construction of such a configuration may arise are ingenuously overcome. The IPS consists of a buoy rigidly connected to a fully submerged tube (acceleration tube), open at both ends, inside which a piston slides. The energy is converted from the relative motion between the floater-tube system and the piston, to the inertia of which the inertia of the water enclosed in the tube is added.

In the present paper, frequency-domain analysis is applied to a specific geometry of the original IPS buoy device concept. Although frequency domain analysis does not allow considering non-linear configurations, which would be the most realistic scenario for the majority of wave power devices, it is particularly useful in the early development stages to establish the response of power take-off mechanism characteristic parameters to different frequencies of the wave power spectrum (e.g. [5]). Optimal mechanical damping and spring coefficients are computed for some parameters restrictions. Absorbed power, capture width and other variables, such as relative displacement, are computed for regular waves and these optimal mechanical coefficients.

Stochastic models are being increasingly applied in wave energy devices' development. Such models were initially established for OWC power plants [6]. A stochastic model is here developed in order to evaluate the IPS buoy behaviour for more realistic irregular waves' conditions. In [7] a simplified stochastic approach was applied to the IPS wave energy converter bringing to light issues concerning inferior device's performance in irregular waves. The stochastic modelling allows for defining probability density functions for relevant parameters that characterize the device's behaviour. In fact, assuming that the overall system behaviour is linear and that the surface elevation for irregular waves may be

regarded as a stochastic process with a Gaussian probability density function, the variables that define the system behaviour, such as the displacements and velocities of the bodies, will also hold a Gaussian probability density function. The average power extraction is then computed for different sea state conditions.

A variation of the original concept, the sloped IPS buoy, in which the buoy-tube system is set to oscillate at an angle intermediate between heave and surge directions, is studied in [8]. Starting from the mid 1990's, numerical and physic models of this configuration have been studied in the University of Edinburgh ([9], [10]). Aiming to enhance the device's hydrodynamic performance, an alternative non-axisymmetric IPS geometry is conceived in the paper. Using the stochastic modelling approach, the device's behaviour is studied for several wave directions and compared to the axisymmetric configuration's behaviour.

II. MATHEMATICAL FORMULATION

In the modelling of the IPS buoy device the floater-tube set will be referred to as body 1 and the piston will be referred to as body 2. It will be assumed that both bodies have linear hydrodynamic behaviour. Two oscillating modes will be assumed for the system: a heave mode for body 1, z_1, and a heave mode for body 2, z_2.

A. Frequency-Domain

Frequency domain analysis does not allow considering non-linear power take-off configurations. This, however, is the most realistic scenario for the majority of wave power devices. For the IPS buoy, in particular, a hydraulic circuit, as in [11], should be considered. This includes a cylinder, high-pressure and low-pressure gas accumulators and a hydraulic motor, as shown in Fig. 1 a). The relative motion between the two bodies induces the displacement of the piston inside the cylinder. A rectifying valve assures that the liquid always enters the high-pressure accumulator and leaves the low-pressure accumulator, and not otherwise, whether the relative displacement between bodies is made downwards or upwards. The resulting pressure difference between the accumulators drives the hydraulic motor.

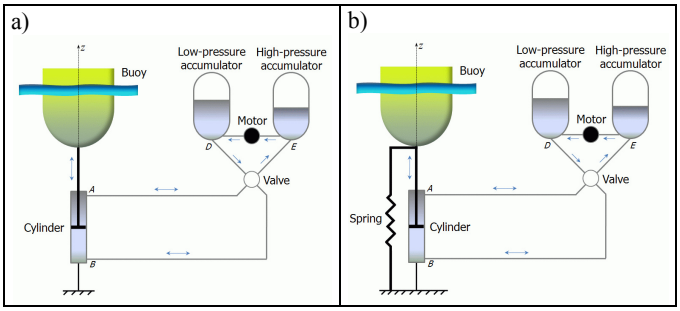

Fig. 1 Schematic representation of the power take-off mechanism consisting of a hydraulic circuit a) with no spring and b) with an additional spring term

It will be here assumed that the hydraulic circuit may be represented by a damping term. In the case in which a spring term is also considered, it is assumed that a parallel spring is added to the hydraulic circuit, as seen in Fig. 1 b). Assuming this last configuration, in which the spring and damping terms are proportional to the relative displacement and to the relative velocity between bodies, respectively, according to Newton's second law the governing equations for the device are expressed in the frequency domain by

$$\begin{aligned} &-M_1\omega^2\hat{z}_1 = F_{d_1} + (\omega^2 A_{11} - i\omega B_{11})\hat{z}_1 + \\ &+(\omega^2 A_{12} - i\omega B_{12})\hat{z}_2 - C_1\hat{z}_1 + (K_L + i\omega D_L)(\hat{z}_2 - \hat{z}_1) \end{aligned}, \tag{1}$$

$$\begin{aligned} &-M_2\omega^2\hat{z}_2 = F_{d_2} + (\omega^2 A_{22} - i\omega B_{22})\hat{z}_2 + \\ &+(\omega^2 A_{21} - i\omega B_{21})\hat{z}_1 - (K_L + i\omega D_L)(\hat{z}_2 - \hat{z}_1) \end{aligned}. \tag{2}$$

Here ω is the angular frequency, $\hat{z}_i$ is the complex displacement amplitude for body i, M_i the mass of body i, C_i the hydrostatic restoring coefficient for body i, A_{ij} and B_{ij} the added mass and damping hydrodynamic coefficients, F_{d_i} the complex amplitude for the diffraction force on body i, and K_L and D_L the spring and damping coefficients of the power take-off equipment.

Following [12], the time averaged power extracted from a wave with angular frequency ω is given by

$$\overline{P} = \frac{1}{2} D_L \omega^2 \left|\hat{z}_2 - \hat{z}_1\right|^2 . \tag{3}$$

The capture width, λ_c, is

$$\lambda_c = \frac{\overline{P}}{\overline{P_i}} = \frac{2D_L\omega^3\left|\hat{z}_2 - \hat{z}_1\right|}{\rho g^2 \left|\hat{A}(\omega)\right|^2 \left(1 + \frac{2kh}{\sinh(2kh)}\right)\tanh(kh)}, \tag{4}$$

where $\overline{P_i}$ is the time averaged power for an incident regular wave with angular frequency ω and complex elevation amplitude $\hat{A}(\omega)$. ρ is the water specific mass, g the acceleration of gravity, h the water depth and k is the wave number given by the positive root of the dispersion relationship $\omega^2/g = k\tanh(kh)$.

B. Stochastic

As in [6], let it be assumed that the sea surface elevation, $\eta(t)$, is a Gaussian random variable in a time interval T, given by

$$\eta(t) = \sum_{n=-\infty}^{+\infty} \hat{A}_n \exp(in\omega_0 t), \tag{5}$$

where $\omega_0 = 2\pi/T$ and $\hat{A}_n = |\hat{A}_n| \exp(i\varphi_n)$ is a complex random variable ($\varphi(n)$ is a random variable uniformly distributed in the interval $[0,2\pi[$). Let it equally be assumed

that $E\left\{\left|\hat{A}_n\right|^2\right\}=\sigma_n^2$ and $E\left\{\hat{A}_n\hat{A}_{n'}^*\right\}=0$ (for $n\neq n'$), in which $E\{\ \}$ represents the expected value.

Assuming that the sea state can be represented by a discrete power spectrum, the variance of the sea surface elevation is, according to [6], defined by

$$\sigma_\eta^2=E\left\{\eta\eta^*\right\}=\sum_{n=-\infty}^{+\infty}\sum_{n'=-\infty}^{+\infty}\exp\left(i(n-n')\omega_0 t\right)E\left\{\hat{A}_n\hat{A}_{n'}^*\right\}=\sum_{n=-\infty}^{+\infty}\sigma_n^2 . \quad (6)$$

For a continuous power spectrum the variance of the sea surface elevation is given by

$$\sigma_\eta^2=\int_{-\infty}^{+\infty}S_\eta(\omega)d\omega, \quad (7)$$

in which $S_\eta(\omega)$ is the spectral density defined in $]-\infty,+\infty[$. Thus, in the limiting case $T\to\infty$ it will be $\omega_0\to d\omega$ and $E\left\{\left|\hat{A}_n\right|^2\right\}=\sigma_n^2\to S_\eta(\omega)d\omega$.

Transfer functions, $HG_1(n\omega_0)$ and $HG_2(n\omega_0)$, relating the amplitude of the incident wave $\hat{A}_n$ to the displacement amplitudes for body 1 and for body 2, may be obtained from equations (1) and (2), so that

$$\hat{z}_1(n\omega_0)=HG_1(n\omega_0)\hat{A}_n \quad (8)$$

and

$$\hat{z}_2(n\omega_0)=HG_2(n\omega_0)\hat{A}_n . \quad (9)$$

Thus, assuming that (5) holds, the vertical displacements for both bodies are given by

$$z_1(t)=\sum_{n=-\infty}^{+\infty}HG_1(n\omega_0)\hat{A}_n\exp(in\omega_0 t) \quad (10)$$

and

$$z_2(t)=\sum_{n=-\infty}^{+\infty}HG_2(n\omega_0)\hat{A}_n\exp(in\omega_0 t). \quad (11)$$

It should be stressed that, like η, z_1 and z_2 are Gaussian random variables, with variances

$$\sigma_{z_1}^2=E\left\{z_1z_1^*\right\}=\sum_{n=-\infty}^{+\infty}\left|HG_1(n\omega_0)\right|^2\sigma_n^2 \quad (12)$$

and

$$\sigma_{z_2}^2=E\left\{z_2z_2^*\right\}=\sum_{n=-\infty}^{+\infty}\left|HG_2(n\omega_0)\right|^2\sigma_n^2 . \quad (13)$$

If a continuous power spectrum is to be assumed, the variances are given by

$$\sigma_{z_1}^2=\int_{-\infty}^{+\infty}S_\eta(\omega)\left|HG_1(\omega)\right|^2 d\omega \quad (14)$$

and

$$\sigma_{z_2}^2=\int_{-\infty}^{+\infty}S_\eta(\omega)\left|HG_2(\omega)\right|^2 d\omega . \quad (15)$$

For the load force f_L given by

$$f_L(t)=\pm\sum_{n=-\infty}^{\infty}(K_L+in\omega_0 D_L)\left(\hat{z}_2(n\omega_0)-\hat{z}_2(n\omega_0)\right)\exp(in\omega_0 t), \quad (16)$$

knowing that $E\left\{\left(\hat{\xi}_1-\hat{\xi}_2\right)_n\left(\hat{\xi}_1-\hat{\xi}_2\right)_{n'}\right\}=0$ for $n\neq n'$ and basing on equations (10) and (11), the variance is

$$\sigma_{f_L}^2=\sum_{n=-\infty}^{+\infty}\left|Z_L(n\omega_0)\right|^2\left|HG_2(n\omega_0)-HG_1(n\omega_0)\right|^2\sigma_n^2 , \quad (17)$$

where $Z_L(n\omega_0)=K_L+in\omega_0 D_L$. In the limiting case of a continuous power spectrum this expression turns into

$$\sigma_{F_L}^2=\int_{-\infty}^{+\infty}S_\eta(\omega)\left|Z_L(\omega)\right|^2\left|HG_2(\omega)-HG_1(\omega)\right|^2 d\omega . \quad (18)$$

The average absorbed power is obtained from

$$\overline{P}=D_L E\left\{\dot{z}_2(t)-\dot{z}_1(t)\right|^2\}, \quad (19)$$

where $\dot{z}_i$ is the vertical velocity of body *i* and, in the limiting case of a sea state represented by a continuous power spectrum,

$$E\left\{\dot{z}_2-\dot{z}_1\right|^2\}=E\left\{(\dot{z}_2-\dot{z}_1)(\dot{z}_2-\dot{z}_1)^*\right\}=$$
$$=\int_{-\infty}^{+\infty}S_\eta(\omega)\omega^2\left|HG_2(\omega)-HG_1(\omega)\right|^2 d\omega . \quad (20)$$

III. NUMERICAL RESULTS

A. Frequency-Domain – Regular Waves

An axisymmetric geometry of the IPS buoy device, corresponding to the original concept, was initially considered. Fig. 2 presents the panel grid describing the wetted surface of this geometry. The piston (body 2) is enclosed in the acceleration tube.

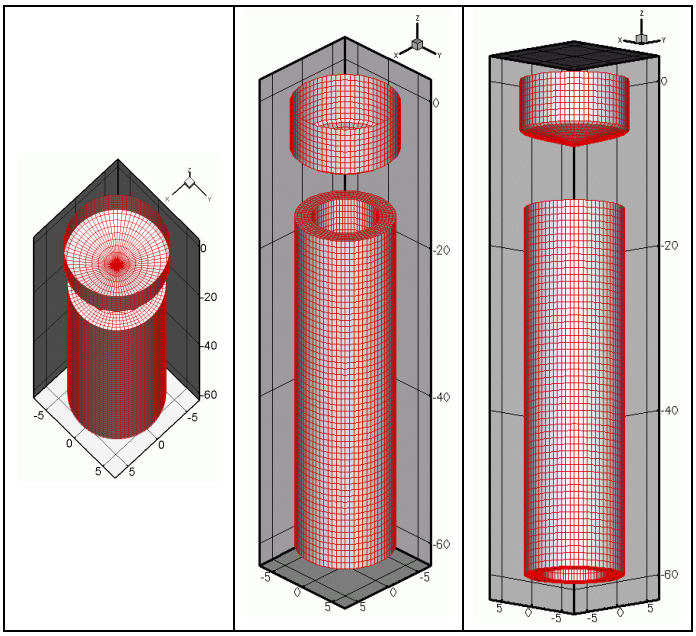

Fig. 1 Three perspectives of the panel grid describing the wetted surface of the IPS buoy axisymmetric geometry

For this geometry, using WAMIT©, hydrodynamic diffraction and radiation coefficients were obtained for a set of 441 wave frequencies in the range of 0.15 rad/s to 2.0977 rad/s. An 80m water depth was assumed.

In an initial linear configuration adopted for the power take-off equipment it is assumed that it can be simulated solely by a damping term (K_L=0). The optimal D_L value which maximizes the absorbed power (hence the capture width λ_c) was computed for each frequency ω (wave period T).

Results refer to 1m amplitude incident regular waves. To avoid unrealistic solutions (body oscillation amplitudes not small compared with body dimensions) falling out of the scope of linear hydrodynamic theory, some restrictions were considered with respect to the amplitude of the heave motion of body 1 and the amplitude of the relative heave motion between the two bodies, $|\hat{z}_2-\hat{z}_1|$. In all the cases it is assumed that the absolute displacement amplitude for body 1 cannot exceed 8m. It is also considered that the amplitude for the relative displacement between body 1 and body 2 cannot exceed 6 and 8m. Thus the case "6_8" means that the amplitude for the relative displacement cannot exceed 6m and the amplitude for the absolute displacement of body 1 cannot be greater than 8m.

Figure 3 presents the dimensionless absorbed power, defined by $\overline{P}^*=\overline{P}/\overline{P}_{\max}$, in which $\overline{P}$ is given by Eq. (3) and $\overline{P}_{\max}$ is the theoretical maximum limit for the time-averaged power that an axisymmetric heaving wave energy converter can absorb from regular waves with frequency ω and amplitude A_w , $\overline{P}_{\max}=\rho g^3 A_w{}^2/(4\omega^3)$ [12]. The two curves correspond to different displacement amplitude restrictions, meaning that, as above mentioned, the first number in the caption refers to the maximum relative vertical displacement (6m and 8m) and the second to the maximum absolute vertical displacement for body 1 (8m in the two scenarios). Bearing in mind that the averaged absorbed power is given by Eq. (3), the first $\overline{P}^*$ peak (around T=11.5s), which corresponds to resonance, should be related to higher relative vertical displacement amplitudes (Fig. 5) and the second (around T=14.5s) to higher optimal D_L values (Fig. 4). In the first peak approximately 73% of $\overline{P}_{\max}$ is reached for 8m maximum $|\hat{z}_1|$ ($\overline{P}$=1107.5kW , λ_c=23.4m). In the second, $\overline{P}$ represents approximately 33% of $\overline{P}_{\max}$ ($\overline{P}$=1061.3kW , λ_c=16.2m) (Fig. 3). The value of the absorbed power depends on the maximum relative vertical displacement amplitude only in the vicinity of T=11.5s - to higher maximum $|\hat{z}_2-\hat{z}_1|$ values correspond higher $\overline{P}$ values (Figures 3 and 5). It is in this wave period range that the highest $|\hat{z}_2-\hat{z}_1|$ values occur, being limited according to the imposed restrictions (Fig. 5). D_L is highly sensitive to wave period, ranging, for 8m maximum $|\hat{z}_1|$, between a value of D_L=94.3kNs/m for T=11.2s and a value of D_L=8932.3 kNs/m in the vicinity of the second $\overline{P}^*$ peak (Fig. 4). Note that in this power take-off configuration $\overline{P}$ is optimized, for each wave period, as a function of D_L , the value of which should simultaneously ensure the effectiveness of the restrictions imposed on the bodies' displacement amplitudes.

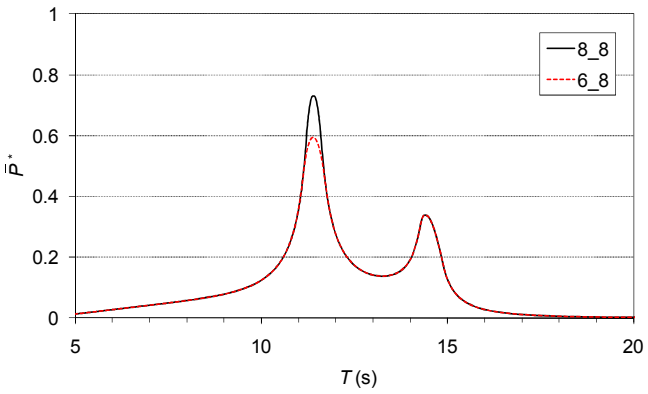

Fig. 3 Dimensionless time averaged absorbed power for 6m and 8m maximum displacement amplitude between body 1 and body 2 (for a 1m amplitude incident regular wave) and 8m maximum absolute displacement amplitude for body 1, assuming the power take-off mechanism simulated by a damping term (in the two displacement amplitude restrictions captions X_Y means (in meters) X = maximum $|\hat{z}_2-\hat{z}_1|$, Y = maximum $|\hat{z}_1|$)

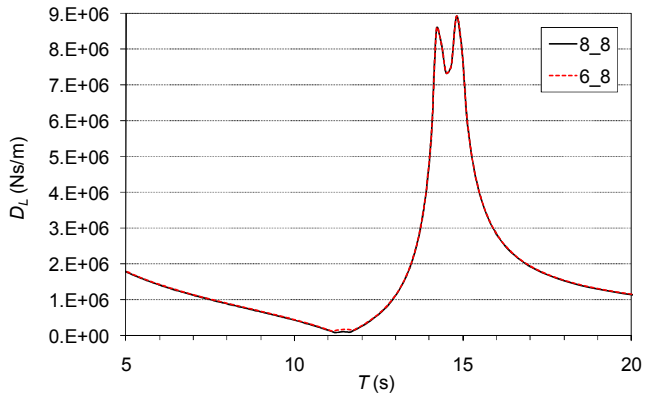

Fig. 4 Mechanical damping coefficient for 6m and 8m maximum displacement amplitude between body 1 and body 2 (for a 1m amplitude incident regular wave) and 8m maximum absolute displacement amplitude for body 1, assuming the power take-off mechanism simulated by a damping term (in the two displacement amplitude restrictions captions X_Y means (in meters) X = maximum $\left|\hat{z}_2-\hat{z}_1\right|$, Y = maximum $\left|\hat{z}_1\right|$)

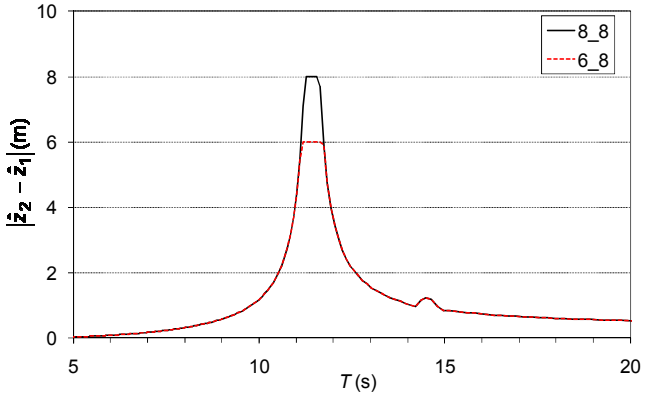

Fig. 5 Relative vertical displacement amplitude, restricted to 6m and 8m, for a 8m maximum absolute displacement amplitude for body 1 (for a 1m amplitude incident regular wave), assuming the power take-off mechanism simulated by a damping term (in the two displacement amplitude restrictions captions X_Y means (in meters) X = maximum $\left|\hat{z}_2-\hat{z}_1\right|$, Y = maximum $\left|\hat{z}_1\right|$)

The second linear configuration assumes power take-off (PTO) equipment simulated by both damping and spring terms. In this case optimal mechanical damping D_L and spring K_L coefficients which maximize the absorbed power (hence the capture width λ_c) are obtained for each frequency ω (wave period T). Restrictions are now imposed only to the amplitude of the relative heave motion between the two bodies, namely 6m and 8m maximum $\left|\hat{z}_2-\hat{z}_1\right|$.

From the observation of Fig. 6, which plots the dimensionless time averaged absorbed power, it is inferred that reactive phase control ($K_L\neq 0$) significantly improves device's performance for a wide range of wave periods ($\overline{P}$ goes up to 3527.3kW for T=15s - λ_c=51.5m). It should be noted, however, that results presented for this PTO configuration consider no absolute displacement amplitude restrictions. For the wave periods T in which the respective restrictions to $\left|\hat{z}_2-\hat{z}_1\right|$ are not active (Fig. 9), absorbed power values reach $\overline{P}_{\max}$ (Fig. 6). Outside this range of periods, $\overline{P}^*$ values for 8m maximum $\left|\hat{z}_2-\hat{z}_1\right|$ are higher than $\overline{P}^*$ values for 6m maximum $\left|\hat{z}_2-\hat{z}_1\right|$ (Fig. 6).

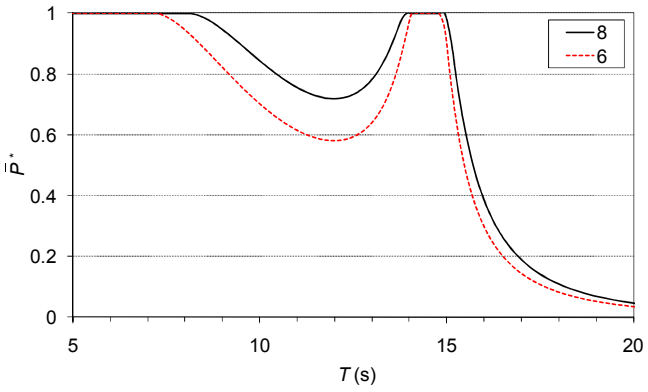

Fig. 6 Dimensionless time averaged absorbed power for 6m and 8m maximum relative vertical displacement amplitudes (for a 1m amplitude incident regular wave), assuming the power take-off mechanism simulated by both damping and spring terms

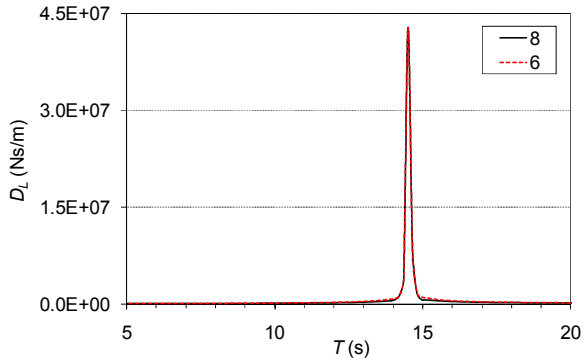

Fig. 7 Mechanical damping coefficient for 6m and 8m maximum relative vertical displacement amplitudes (for a 1m amplitude incident regular wave), assuming the power take-off mechanism simulated by both damping and spring terms

The maximum mechanical damping coefficient D_L=42814.5 kNs/m (nearly 5 times superior to maximum D_L in the previous configuration - Fig. 4) corresponds to T=14.5s (Fig. 7). In the same wave period the amplitude of the relative heave motion and the mechanical spring coefficient present minimum values $\left|\hat{z}_2-\hat{z}_1\right|$=0.9m (Fig. 9) and K_L=-15619.3 kN/m (Fig. 8). Maximum value K_m=10680.3 kN/m is reached in adjacent wave period T=14.7s (Fig. 8). In this PTO configuration the imposition of restrictions to $\left|\hat{z}_2-\hat{z}_1\right|$ is determined by adequate values of

both D_L and K_L. The admissible domain of values for D_L is, in this scenario, $D_L \in [149, 42814.5]$(kNs/m) for 8m maximum $|\hat{z}_2 - \hat{z}_1|$. As for the mechanical spring, negative stiffness values are only interesting from a conceptual point of view. Bearing that in mind, admissible values are here comprehended in the interval $K_L \in [0, 10680.3]$(kN/m).

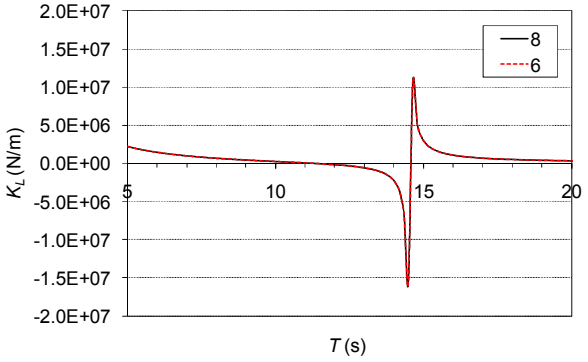

Fig. 8 Mechanical spring coefficient for 6m and 8m maximum relative vertical displacement amplitudes (for a 1m amplitude incident regular wave), assuming the power take-off mechanism simulated by both damping and spring terms

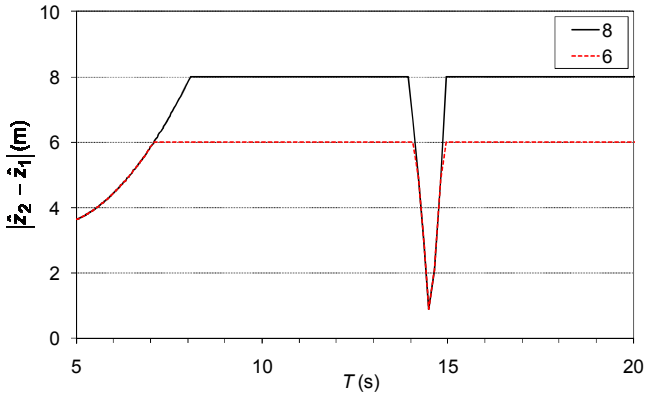

Fig. 9 Relative vertical displacement amplitude, restricted to 6m and 8m, for a 1m amplitude incident regular wave, assuming the power take-off mechanism simulated by both damping and spring terms

B. Stochastic Model

In reality sea waves are random and irregular, therefore more suitable to a stochastic modelling. This does not allow for the planning of control strategies but should provide a more realistic assessment of the device's performance in real conditions, without the need to resort to the complexity of a time domain analysis.

Stochastic modelling is initially applied to the geometry represented in Fig. 2. The same set of hydrodynamic diffraction and radiation coefficients used for regular waves was considered. Following the theoretical modelling in section II, incident waves are now described by a frequency spectrum. The adopted Pierson-Moskowitz formulation (see [13]), expressed in terms of the sea state's significant wave height H_s and energy period T_e, is

$$S_\eta(\omega) = 263 H_s^2 T_e^{-4} \omega^{-5} \exp\left(-1054 T_e^{-4} \omega^{-4}\right). \quad (21)$$

The same two PTO linear configurations considered for regular waves are considered: 1) simulated solely by a damping term (K_L=0); 2) simulated by both damping and spring terms. The values of K_L and D_L that maximize the averaged absorbed power given by Eq. (19) are obtained for each sea state. Fig. 10 presents for the two PTO configurations the absorbed power $\overline{P}$ (above) and the dimensionless absorbed power $\overline{P}^* = \overline{P}/\overline{P}_{\max}$ (below). Here $\overline{P}$ is given by Eq. (19) and the maximum power extractable from a sea state represented by the spectral distribution $S_\eta(\omega)$ by a heaving axisymmetric body is $\overline{P}_{\max} = \frac{g^3 \rho}{4} \int_0^\infty \omega^{-3} S_\eta(\omega) d\omega = 149.5 H_s^{\,2} T_e^{\,3}$ (see [7]). Sea states with H_s=2m and T_e ranging from 7 to 16s are considered. For a PTO mechanism simulated by a damping term the device performs better in a sea state with H_s=2m and T_e=9s (although the highest dimensional value $\overline{P}$=79.6kW occurs to T_e=11s - λ_c=3.4m) (Fig. 10, black diamonds). Nevertheless only about 15% of $\overline{P}_{\max}$ is reached. This represents a significant performance decay comparing to what is observed in regular waves (Fig. 3), a problematic widely discussed in recent works (see [3]). The improvements achieved by adding a spring to the PTO mechanism prove to be generally marginal (highest dimensional value $\overline{P}$=84.3kW occurs to T_e=11s - λ_c=3.6m) (Fig. 10, red squares). In fact, only for sea states with T_e=7s and T_e=8s $\overline{P}^*$ values are clearly higher in the second PTO configuration (approximately 2 times higher for T_e=7s).

Figures 11 and 12 present the dimensionless optimal mechanical damping and spring coefficients, D_L^* and K_L^*. These are obtained from $D_L^* = D_L / B(T_{11.5})$ and $K_L^* = K_L / \rho g S$, in which $B(T_{11.5})$=37.4kNs/m is body 1's hydrodynamic damping coefficient for T=11.5s and $\rho g S$=1334.2 kN/m (S is the cross sectional area of body 1). Minimum (negative) K_L^* values occur for sea states with T_e=13s and T_e=14s (Fig. 12) (-847.4 kN/m $\le K_L \le$ 1337.3 kN/m). In these same energy periods the most significant differences between D_L^* values for the two PTO configurations are observed - D_L^* values for the first configuration (K_L=0, 202 kNs/m $\le D_L \le$ 6057.8 kNs/m) are considerably higher than the values for the second configuration ($K_L \neq 0$, 126.7 kNs/m $\le D_L \le$ 4923.2 kNs/m) (Fig. 11). In general the highest D_L^* values refer to the energy periods in which $|K_L^*|$

values are higher. Naturally, the lower the $|K_L^*|$ value, the less significant is the difference between D_L^* values for the two PTO configurations (the limiting case being $|K_L^*|=0$).

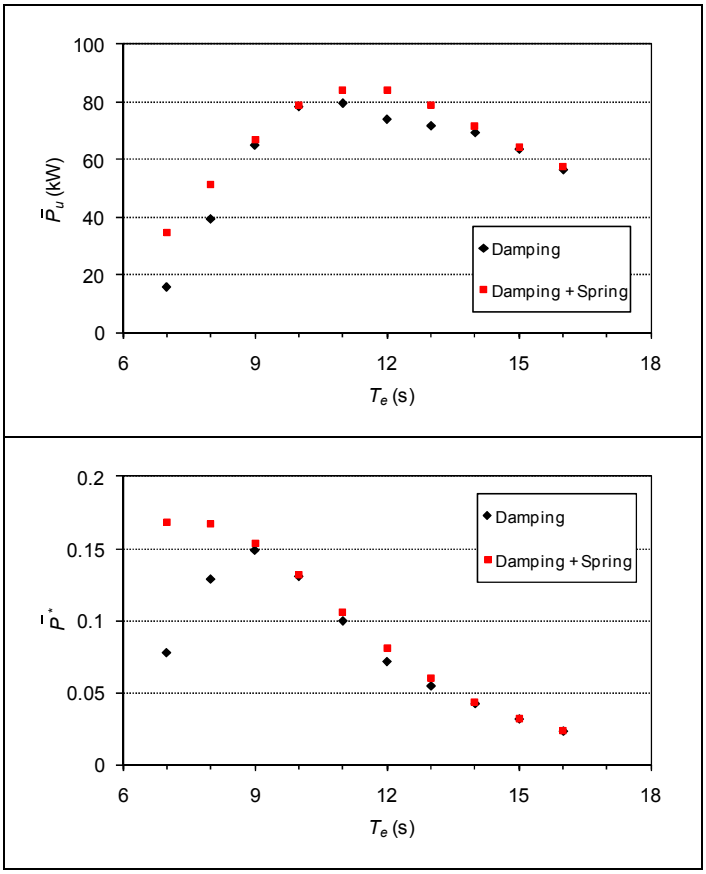

Fig. 10 Time averaged absorbed power (above) and dimensionless time averaged absorbed power (below) for H_s=2m and T_e=7–16s , assuming the power take-off mechanism simulated by a damping term and assuming the power take-off mechanism simulated by both damping and spring terms

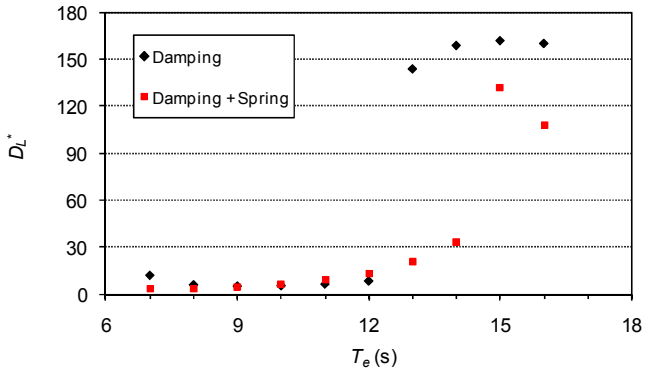

Fig. 11 Dimensionless mechanical damping coefficient for H_s=2m and T_e=7–16s , assuming the power take-off mechanism simulated by a damping term and assuming the power take-off mechanism simulated by both damping and spring terms

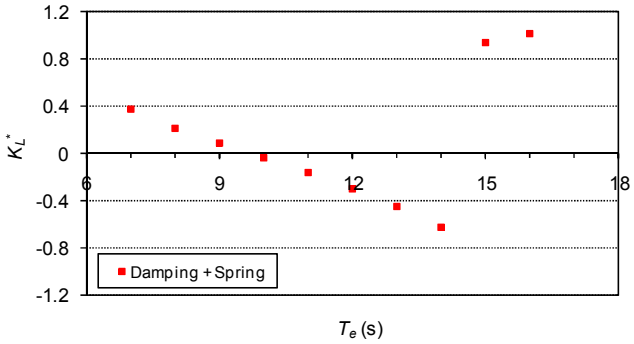

Fig. 12 Dimensionless mechanical spring coefficient for H_s=2m and T_e=7–16s , assuming the power take-off mechanism simulated by damping and spring terms

Some variations of the original IPS concept have been proposed. Notable are the cases of the modified version introduced by the inventor to limit the stroke of the piston [14], Aquabuoy, which combines IPS buoy concept with hose pump technology [15], and the sloped IPS buoy [8]. According to [16], two-dimensional symmetric systems oscillating in a single mode radiate similar waves in opposite directions, so that no more than 50% of the incident energy can be absorbed. Absorption levels superior to 50% may essentially be achieved in two ways: i) by considering two-dimensional symmetric systems oscillating in a combination of either surge and heave or pitch and heave; ii) by considering two-dimensional systems with non-symmetric radiating characteristics. The latter is the case of Salter's Duck, a pitch oscillator, which has revealed in tests absorbed power levels superior to 80% of the incident power [17].

With a view to improving the device's hydrodynamic performance, an alternative configuration for the IPS buoy is here proposed, in which an element connecting the floater to the tube is introduced to break its symmetry. Panel grid describing the wetted surface of this non-axisymmetric geometry is presented in Fig. 13.

As in the previous case, hydrodynamic diffraction and radiation coefficients for a set of 441 wave frequencies in the range 0.15-2.0977 rad/s (and different incidence directions, in the present case) were obtained for this geometry, using WAMIT©. Again an 80m water depth was assumed. The same two linear configurations are here adopted for the power take-off equipment: 1) simulated solely by a damping term (K_L=0); 2) simulated by both damping and spring terms.

Results are presented for sea states with H_s=2m , T_e ranging from 7 to 16s and incidence direction of 0º, 45º and 90º (it is assumed that 0º corresponds to surge direction). Fig. 14 shows the time averaged absorbed power for a PTO mechanism simulated by a damping term. The pattern of the curves for the different incidence directions is fairly similar. In the three cases the highest $\bar{P}$ value occurs for T_e=11s . Except for T_e=13s , absorbed power levels for a 0º direction

are higher ($\overline{P}(T_e$=11s)=79.0kW , λ_c=3.4m). Nevertheless, differences between these and $\overline{P}$ levels for 45º and 90º directions are inferior to 5%, which proves the reduced device's response in relation to incident direction. In relation to the axisymmetric IPS configuration, no significant changes in performance are observed for this linear damper PTO configuration (with no spring): the highest absorbed power value in the present case, $\overline{P}(T_e$=11s)=79.0kW for 0º direction, is inferior in about 1% to the highest for the axisymmetric configuration ($\overline{P}(T_e$=11s)=79.6kW).

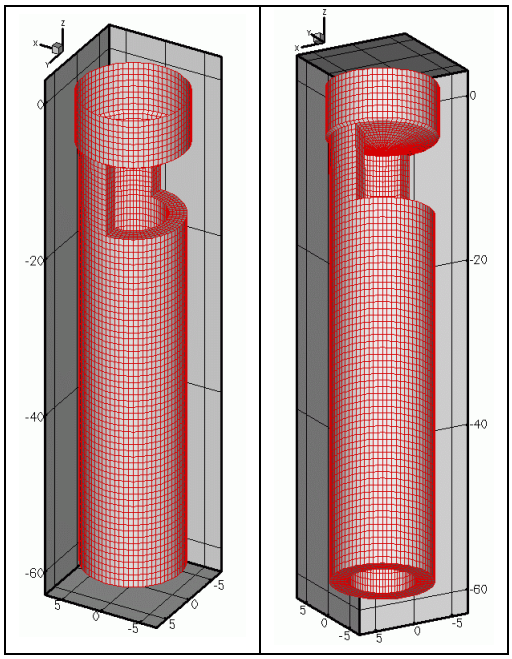

Fig. 13 Two perspectives of the panel grid describing the wetted surface of the IPS buoy non-axisymmetric geometry

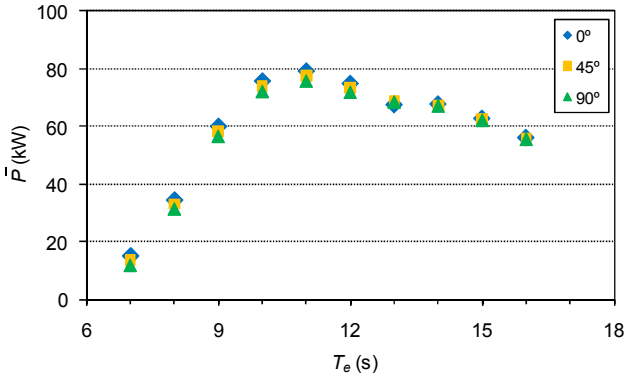

Fig. 14 Time averaged absorbed power for H_s=2m , T_e=7–16s and 0º, 45º and 90º incidence direction, assuming the power take-off mechanism simulated by a damping term

When it comes to the second PTO configuration (simulated by damping and spring terms), the device's performance shows a greater dependence from the direction of incidence (Fig. 15), in particular for sea states with lower wave energy period (T_e≤9s). The relative difference between the $\overline{P}$ value for 0º and the $\overline{P}$ value for 90º is about 8% for T_e=9s and 27% for T_e=7s . However, for the wave energy periods in which the higher $\overline{P}$ levels occur the relative differences are inferior to 5%. The highest absorbed power level in this case $\overline{P}(T_e$=12s)=81.5kW (λ_c=3.1m) (for 0º incidence direction), corresponds to approximately 97% of the highest value obtained for the axisymmetric configuration ($\overline{P}(T_e$=11s)=84.3kW).

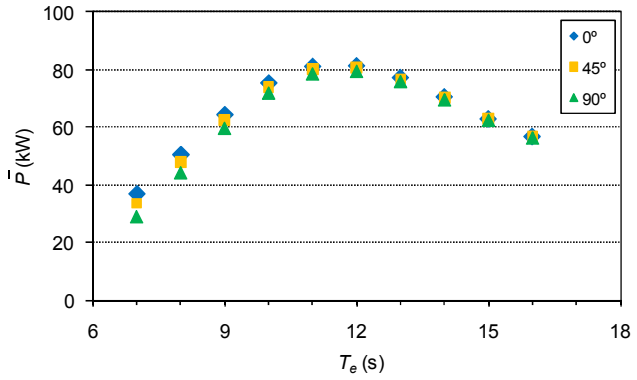

Fig. 15 Time averaged absorbed power for H_s=2m , T_e=7–16s and 0º, 45º and 90º incidence direction, assuming the power take-off mechanism simulated by damping and spring terms

Figures 16 to 18 present the dimensionless optimal mechanical damping and spring coefficients, D_L^* and K_L^*, for the two considered PTO configurations. Again $D_L^*=D_L/B(T_{11.5})$ and $K_L^*=K_L/\rho gS$, with the hydrodynamic damping coefficient of body 1 for T=11.5s $B(T_{11.5})$=34.2kNs/m and, as in the axisymmetric geometry's case (the cross sectional area of body 1, S, is the same), ρgS=1334.2 kN/m . The curves referring to the two PTO configurations in the non-axisymmetric IPS version (Figures 16 to 18) generally present significant similarities with the curves in the axisymmetric version (Figures 11 and 12). However, note that, for a sea state with T_e=13s and a 0º incidence direction, the non-axisymmetric IPS assuming a PTO mechanism with no spring behaves differently from what is observed for the other directions and from what is observed for the axisymmetric version. In fact, D_L^* (215.7 kNs/m ≤ D_L ≤ 5986.5 kNs/m for 0º direction) presents, for this wave energy period and direction, a value considerably lower than the ones verified for 45º and 90º (Fig. 16) and the one verified for the axisymmetric version (Fig. 11). However, $\overline{P}$ levels for T_e=13s are similar ($\overline{P}(T_e$=13s)=71.7kW for the axisymmetric version), which means that, taking into consideration that the absorbed power

is obtained from Eq. (19), a higher $|\dot{z}_2(t)-\dot{z}_1(t)|^2$ mean value corresponds to 0º direction. These behaviour fluctuations should be related to the positioning of the symmetry breaking element in relation to the incoming wave field.

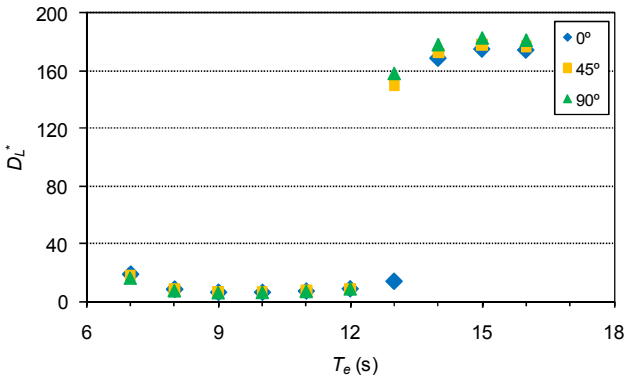

Fig. 16 Dimensionless mechanical damping coefficient for H_s=2m , T_e=7–16s and 0º, 45º and 90º incidence direction, assuming the power take-off mechanism simulated by a damping term

As far as the second PTO configuration is concerned ($K_L \neq 0$), the similarity between the D_L^* and K_L^* curves for the different considered directions is notorious (Figures 17 and 18). The same argumentation is valid when comparing these with the respective curves for the axisymmetric IPS version (Figures 11 and 12). Maximum value D_L=4975.0kNs/m , for T_e=15s and 0º direction, is comparable to the maximum obtained for the axisymmetric IPS, D_L=4923.2kNs/m , also for T_e=15s . Maximum values for 45º and 90º directions are superior to this in 2% and 5%, respectively (131 kNs/m $\leq D_L \leq$ 4975 kNs/m for 0º direction).

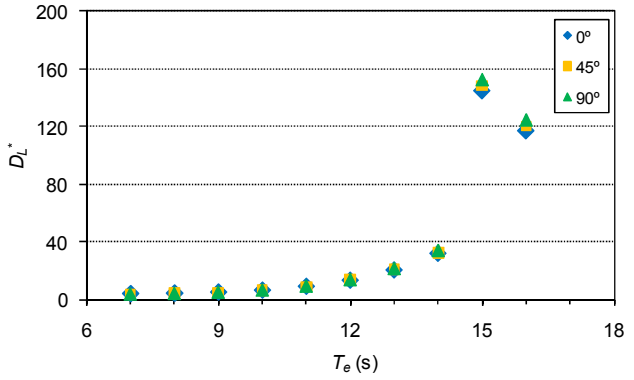

Fig. 17 Dimensionless mechanical damping coefficient for H_s=2m , T_e=7–16s and 0º, 45º and 90º incidence direction, assuming the power take-off mechanism simulated by damping and spring terms

For a 0º incidence direction, the spring coefficient varies between minimum value $K_L(T_e$=14s)=-759.5kN/m and maximum $K_L(T_e$=16s)=1327.4kN/m . Although the minimum value is superior to the one obtained for the axisymmetric IPS ($K_L(T_e$=14s)=-847.4kN/m) in about 12%, the maximum is similar ($K_L(T_e$=16s)=1337.3kN/m). The difference between these and the values obtained for the remaining directions is negligible.

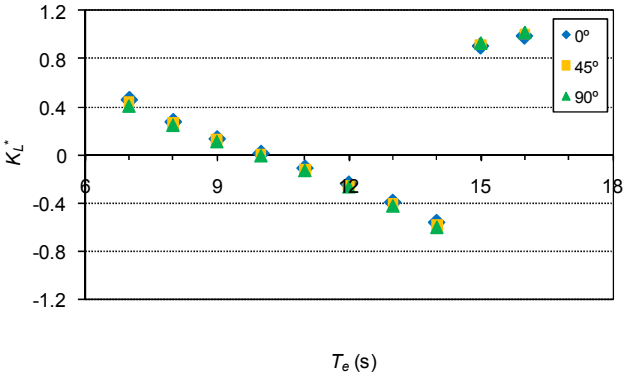

Fig. 18 Dimensionless mechanical spring coefficient for H_s=2m , T_e=7–16s and 0º, 45º and 90º incidence direction, assuming the power take-off mechanism simulated by damping and spring terms

IV. Conclusions

Initially, frequency-domain analysis was applied to the IPS buoy device in its original axisymmetric configuration. Two oscillating modes were considered, namely heave mode for body 1 and heave mode for body 2. In the simulation of the power take-off mechanism two linear configurations were adopted: simulated solely by a damping term and simulated by both damping and spring terms. In each case, the respective optimal mechanical coefficients are obtained. In order to avoid unrealistic solutions falling out of the scope of linear hydrodynamic theory, some restrictions were imposed to the amplitude of the heave motion of body 1 and to the amplitude of the relative heave motion between the two bodies. Absorbed power results for the first PTO configuration (no spring) revealed two distinct peaks. The restrictions imposed to displacements' amplitudes proved to limit energy absorption, so that the theoretical maximum limit is not reached. This condition changes when a spring term is added to the PTO mechanism (reactive phase control), in which case the theoretical maximum is obtained for several wave periods. In any of the two considered PTO configurations the mechanical coefficients proved to be highly sensitive to wave period. The significantly poorer device performance observed in irregular waves (stochastic model) should be related to this circumstance.

With a view to enhancing the device's hydrodynamic performance (particularly having in mind the low absorbed power levels in irregular waves), a new non-axisymmetric IPS geometry was proposed. The stochastic model developed to

evaluate the axisymmetric version's performance in irregular waves was applied to this alternative configuration. Different wave directions were considered. The two linear PTO configurations and the two oscillating modes previously considered were assumed here. It was concluded that, in any of the PTO configurations, absorbed power levels obtained for the different wave directions converge with higher energy period values. In fact, as should be expected, for higher wavelengths the device's behaviour is closer to the characteristics of a point absorber. However, the differences between the results obtained for the different directions are generally negligible. Additionally, the comparison between these and the results for the traditional axisymmetric configuration revealed no significant differences.

ACKNOWLEDGMENT

The work here reported was supported by the Portuguese Foundation for Science and Technology under the contract PTDC/EME-MFE/111763/2009.

REFERENCES

[1] J. Falnes, "Wave-energy conversion through relative motion between two single-mode oscillating bodies", *Journal of Offshore Mechanics and Arctic Engineering*, 121:32-38, 1999.

[2] V. Ferdinande and M. Vantorre M. *The concept of a bipartite point absorber*, in D.V. Evans and A.F. de O. Falcão, Eds., Hydrodynamics of Ocean Wave-Energy Utilization. Berlin, Germany: Springer, 1986, pp. 217–226.

[3] J.J. Cândido and P.A.P.S. Justino, "Modelling, Control and Pontryagin Maximum Principle for a Two-body Wave Energy Device", *Renewable Energy*, Vol. 36, No. 5, pp. 1545-1557, May 2011.

[4] S.A. Noren, "Plant for utilizing kinetic energy", U.S. Patent 4 277 690, 1981. (Original Swedish patent 7808679, 1978.)

[5] A. Clément, A. Babarit, J.C. Gilloteaux, C. Josset and G. Duclos, "The SEAREV wave energy converter", in *Proc. 6th EWTEC 2005*, Glasgow, UK, 2005.

[6] A.F. de O. Falcão and R. Rodrigues, "Stochastic modelling of OWC wave power plant performance", *Applied Ocean Research*, 24:59-71, 2002.

[7] A.F. de O. Falcão, P.A.P. Justino, J.C.C. Henriques and J.M.C.S. André, "Modelling and control of the IPS wave power buoy", in *Proc. 2nd ICOE 2008*, Brest, France, 2008

[8] S.H. Salter and C.P. Lin, "Wide tank efficiency measurements on a model of the sloped IPS buoy", in *Proc. Third European Wave Energy Conference*, Patras, Greece, 1998, pp. 200-206.

[9] G.S. Payne, J.R.M. Taylor, T. Bruce, P. Parkin, "Assessment of boundary-element method for modelling a free-floating sloped wave energy device. Part 1: Numerical modeling", *Ocean Engineering*, 35: 333-341, 2008.

[10] G.S. Payne, J.R.M. Taylor, T. Bruce, P. Parkin, "Assessment of boundary-element method for modelling a free-floating sloped wave energy device. Part 2: Experimental validation", *Ocean Engineering*, 35: 342-357, 2008.

[11] A.F. de O. Falcão, "Modeling and control of oscillating-body wave energy converters with hydraulic power take-off and gas accumulator", *Ocean Engineering*, 34:2021-32, 2007.

[12] J. Falnes, *Ocean waves and oscillating systems*, Cambridge, UK: Cambridge University Press, 2002.

[13] Y. Goda, *Random Seas and Design of Marine Structures*, Tokyo, Japan: University of Tokyo Press, 1985.

[14] S.A. Noren, "Apparatus for recovering the kinetic energy of sea waves", U.S. Patent 4 773 221, 1988. (Original Swedish patent 8104407, 1981).

[15] A. Weinstein, G. Fredrikson, M.J. Parks, K. Nielsen, "AquaBuOY, the offshore wave energy converter - numerical modelling and optimization", in *Proc. MTTS/IEEE Techno-Ocean '04 Conference*, vol. 4, 1854-1859, Kobe, Japan, 2004.

[16] J. Falnes, "Optimum control of oscillation of wave-energy converters", *International Journal of Offshore and Polar Engineering*, 12 (2): 147–155, 2002.

[17] S.H. Salter, D.C. Jeffery, J.R.M. Taylor, "The architecture of nodding duck wave power generators", *The Naval Architect*, 1: 21-24, 1976.